HARDENING OF NICKEL ALLOYS BY ION IMPLANTATION OF TITANIUM AND CARBON

S. M. MYERS, D. M. FOLLSTAEDT, J. A. KNAPP, AND T. R. CHRISTENSON
Sandia National Laboratories, Albuquerque, NM 87185-1056, smmyers@sandia.gov

ABSTRACT

Dual ion implantation of titanium and carbon was shown to produce an amorphous surface layer in annealed bulk nickel, in electroformed Ni, and in electroformed $Ni_{0.75}Fe_{0.25}$. Diamond-tip nanoindentation coupled with finite-element modeling quantified the elastic and plastic mechanical properties of the implanted region. The amorphized matrix, with a thickness of about 100 nm, has an intrinsic hardness near 16 GPa, exceeding by an order of magnitude the value for annealed bulk Ni. Implications for the control of friction and wear in micro-electromechanical systems are discussed.

INTRODUCTION

The performance and lifetime of micro-electromechanical systems (MEMS) fabricated from nickel alloys [1-3] would be enhanced by reductions in sliding friction and wear. It is important, however, that processing to achieve these reductions minimize dimensional changes and heating and avoid the introduction of surfaces layers that are susceptible to debris-forming exfoliation or to degradation with time. Room-temperature alloying by ion implantation satisfies these criteria and, in addition, provides access to metastable phases and tailored nanometer-scale microstructures that exhibit superior mechanical properties [e.g., refs. 4-6]. Previously, ion implantation into Ni was reported to produce hardening and to reduce friction and wear during unlubricated pin-on-disc testing with steel pins [7,8]. The greatest tribological improvements were associated with amorphization, which was achieved by room-temperature implantation of boron or phosphorus or by carbon implantation at cryogenic temperatures.

In the present work we examined the effects of dual implantation of titanium and carbon on the microstructure and mechanical properties of annealed bulk Ni, electroformed Ni, and electroformed $Ni_{0.75}Fe_{0.25}$, the latter two materials being used in MEMS. This implantation treatment was previously applied to steels, and it produced an amorphous layer with exceptionally favorable tribological properties [5], superior in particular to steels amorphized by dual implantation of P and C [9]. We implanted the Ti and C into Ni alloys to concentrations of about 16 at.%. This led to amorphization, paralleling the behavior of steels [4] as well as that of Ni implanted to higher doses of Ti and C [10]. We quantified the elastic and plastic mechanical properties of the amorphized zone by performing diamond-tip indentation testing at penetrations below 1μm, a procedure referred to as nanoindentation, and analyzed the results by finite-element modeling [11,12]. This refined approach, not previously applied to implanted Fe and Ni alloys, indicated order-of-magnitude strengthening by the implantation treatment.

COMPOSITION AND MICROSTRUCTURE

The base materials in this study were of three types: bulk Ni vacuum annealed at 1000°C for 2 hours, unannealed electroformed Ni, and unannealed electroformed $Ni_{0.75}Fe_{0.25}$, the latter two materials being extracted from MEMS processing [3]. Titanium and then C were implanted at room temperature, each to a dose of 2×10^{17} cm^{-2}. The respective implantation energies were

180 and 45 keV, chosen to produce approximate coincidence of the concentration profiles; the corresponding range distributions in pure Ni, calculated using the ion-range code TRIM [13], are plotted in Fig. 1. Also shown is the final depth profile of the Ti as obtained from Rutherford-backscattering spectrometry (RBS) with 2.8 MeV He assuming that the atomic density of the implanted layer is equal to that of crystalline Ni. The Ti and C distributions extend somewhat beyond 100 nm, with the Ti concentration peaking at approximately 16 at.%.

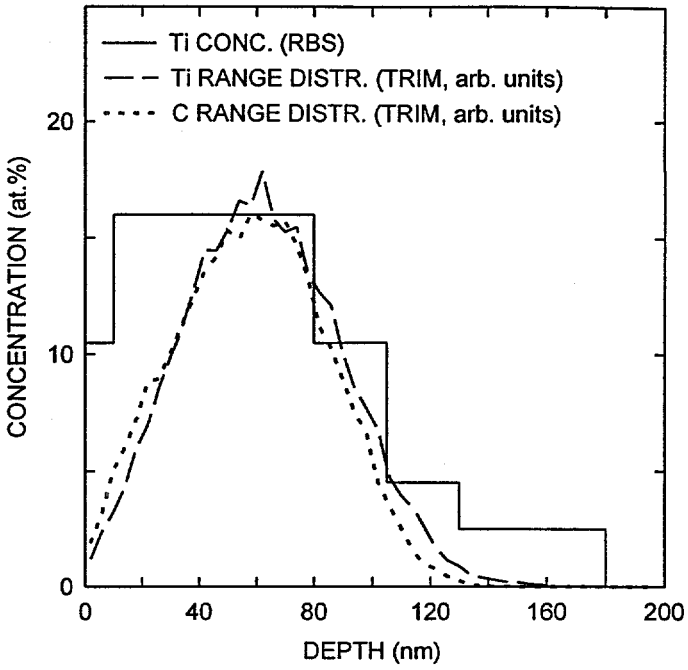

Fig. 1. Titanium depth profile from RBS; Ti and C range distributions from TRIM.

The microstructure produced by implantation is shown in Fig. 2 for the case of electroformed Ni. The plan-view, dark-field image from transmission electron microscopy (TEM) encompasses a wedge-shaped region as depicted schematically; the left-hand portion of this image shows only the amorphous near-surface region, while the right-hand side includes the underlying crystalline matrix with a grain-size range of ~30-600 nm. The presence of the amorphous layer is demonstrated by the diffuse transmission electron diffraction pattern in the lower panel. A similar microstructure was observed in the electroformed $Ni_{0.75}Fe_{0.25}$ alloy. In the case of bulk Ni annealed at 1000°C before implantation, crystalline Ni inclusions 10-40 nm in size were observed within the near-surface region of the amorphous layer.

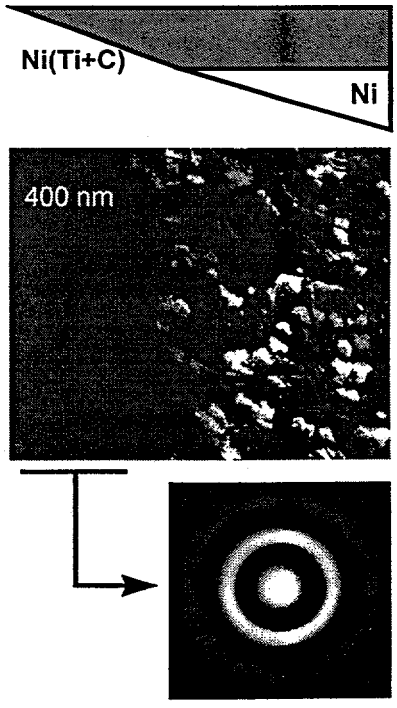

Fig. 2. Microstructure of electroformed Ni implanted with Ti and C.

MECHANICAL PROPERTIES

Nanoindentation testing [14] was performed [15] with a three-sided pyramidal diamond tip (Berkovich indenter). To facilitate quantitative modeling, the area-versus-depth function of the tip was calibrated by indentation of vitreous SiO_2. During testing the tip impinged quasistatically at a constant speed, and the applied force was recorded as a function of penetration depth. Reproducibility was confirmed by performing ten indents on each specimen.

The finite-element modeling of indentation used the commercial code ABAQUS/Standard version 5.5 [16] as detailed elsewhere [11,12]. The diamond tip was modeled as a purely elastic, axisymmetric cone having the area-versus-depth function of the calibrated Berkovich indenter.

The crystalline Ni and $Ni_{0.75}Fe_{0.25}$ matrices were modeled as isotropic elastic-plastic solids using the metal plasticity model in ABAQUS with a Mises yield criterion and a work-hardening rate that conformed to the stress-strain curve for single-crystal Ni [17]. The amorphous layers also were treated as elastic-plastic Mises solids, but in this case work hardening was assumed not to occur, so that the stress-strain curve consisted of a linear elastic segment at low strain joined to a constant-stress plastic region at high strain. These stress-strain curves were adjusted to produce agreement with the experimental data by varying two parameters, Young's elastic modulus and yield stress, the latter being defined as the stress at a plastic strain of 0.002. As these parameters were varied, the work-hardening rates discussed above were held fixed.

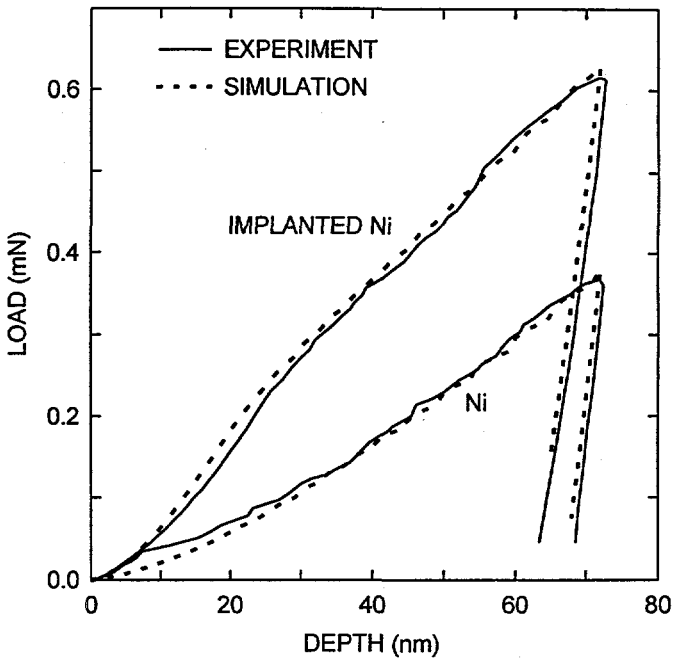

Fig. 3. Data and simulation from indentation tests of unimplanted bulk Ni and bulk Ni implanted with Ti and C.

Indentation data for annealed bulk Ni and for annealed bulk Ni implanted with Ti and C are shown in Fig. 3, together with the fitted simulations. We, like other investigators [8], found that the near-surface region of annealed pure Ni exhibited a higher apparent hardness than the underlying bulk during indentation testing; the origin of this effect is not known but may be related to delayed nucleation of dislocations. Accordingly, the yield stress for the unimplanted specimen was allowed to vary with depth in the simulations. The simulation for the implanted sample retained the mechanical properties of the unimplanted material at depths beyond the implantation-affected zone, but within the implanted region the yield stress and elastic modulus were allowed to vary. The resulting depth profiles of yield stress are shown in Fig. 4. It may be noted that the depth of the strengthened region, as parameterized by the half-amplitude point, extends about 40 nm beyond the half-amplitude Ti concentration in Fig. 3. This greater thickness produced better agreement with the indentation data, and it is justified to a degree by noting that yield strength probably is not proportional to Ti concentration. Similar indentation testing and finite-element modeling of unimplanted and implanted specimens were carried out for electroformed Ni and electroformed $Ni_{0.75}Fe_{0.25}$.

In order to paramaterize the deformation resistance of the near-surface region as realistically as possible, we employed an "intrinsic" hardness. This quantity is defined herein as the asymptotic ratio of force to indentation contact area for an imaginary infinite solid having the mechanical properties of the region of interest in the actual specimen. Such an intrinsic hardness, which is obtained from an auxiliary finite-element calculation, has two useful features: first, it reflects the large-strain behavior of the matrix that tends to dominate surface deformation, in contrast to the yield strength which characterizes only the onset of plasticity; and, second, it reduces to the standard indentation hardness in uniform solids. The concept is illustrated in Fig. 4, where the ratio of force to contact area, or hardness, is plotted versus indenter penetration depth for two simulations: the first is that discussed above for annealed bulk Ni containing an

implanted layer, while the second simulation treats a semi-infinite uniform solid having the properties of the central region of the implanted layer. (Slight oscillations in the simulations arise from the finite size of the discretization elements.) The asymptotic hardness from the latter plot, 16 GPa, is taken to be the intrinsic hardness of the implanted matrix.

The simulation results in Figs. 3 and 4 serve to illustrate the need for finite-element analysis in quantifying by indentation the mechanical properties of thin hard layers on much softer substrates. In structures of this type, indenter penetration is accommodated in large part by pressing the hard overlayer into the soft substrate, even for penetration depths less than one half the layer thickness. As a result, the indentation response is different from that of a uniform solid having the properties of the thin layer, and assuming for simplicity that the two are the same can produce substantial errors. Because of this effect, the order-of-magnitude increase in the near-surface yield stress produced by implantation causes a substantially smaller change in the force-versus-penetration profile in Fig. 3. Moreover, in Fig. 4, the computed hardnesses for the thin implanted layer on Ni and for the uniform matrix with implanted-layer properties are notably different: as a result of substrate deformation, the hardness of the layered structure peaks below that of the uniform matrix and is rapidly decreasing with depth at the middle of the high-strength region.

In Fig. 5, the intrinsic hardness is plotted with Young's elastic modulus for all of the specimens

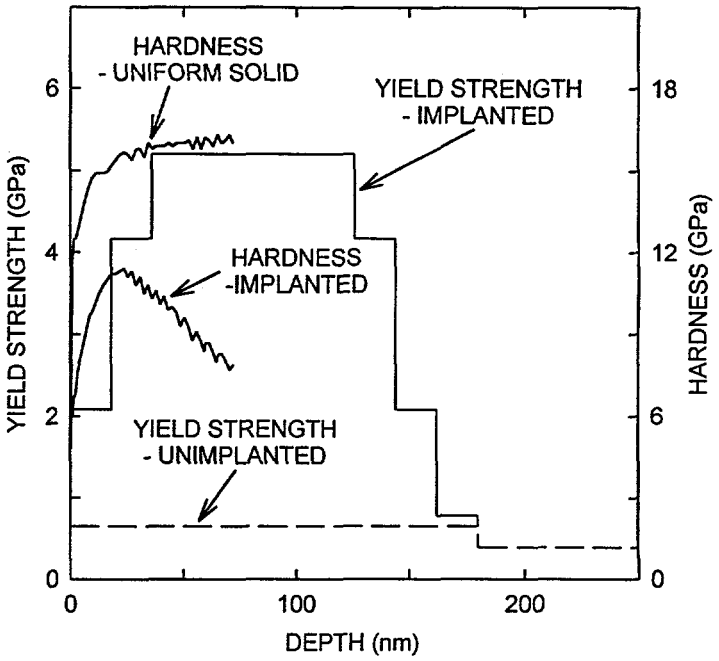

Fig. 4. Depth profiles of the yield stresses used to simulate unimplanted and implanted bulk Ni; computed hardness versus indenter penetration for the implanted sample and for a semi-infinite uniform solid having the properties of the implanted layer.

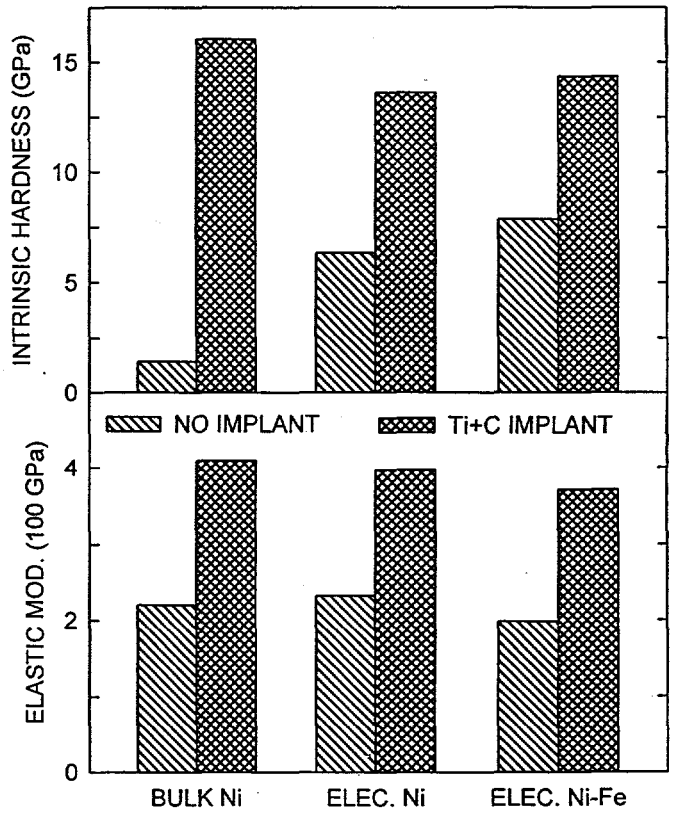

Fig. 5. Intrinsic hardness and elastic modulus of the implanted and unimplanted materials.

evaluated in this work. In the case of the implanted samples, the values correspond to the maximum-strength region of the implanted layer, while for the unimplanted materials, the numbers reflect the asymptotic properties of the bulk matrix. From consideration of the reproducibility of the experimental data and the assumptions made in modeling, we estimate that the absolute uncertainty in the plotted quantities is ±20%. The amorphizing implantations of Ti and C are seen to increase the intrinsic hardness by as much as an order of magnitude.

DISCUSSION AND IMPLICATIONS

Exceptionally high stresses are required to induce plastic flow in amorphous metals [18,19], often ~μ/50 with μ the shear modulus, because deformation by dislocation glide is not operative in the absence of crystallinity [20]. Consistent with this rule of thumb, amorphous Fe-Ni alloys stabilized by metalloid additions generally yield at ~2-3 GPa and exhibit hardnesses of ~7-10 GPa [19]. When the metalloid is C, however, and alloying additions with strong C affinity are introduced, the strength of the amorphous matrix increases still further [21], presumably due to atomic pairing. For example, going from $Fe_{70}Mo_{12}C_{18}$ to $Fe_{68}Ti_2Mo_{12}C_{18}$ was reported to increase the hardness of bulk alloys by about 1 GPa. This suggests that the 16 at.% of Ti in the implanted layers of this work might lead to substantial additional increments of yield strength and hardness. Our finding of 16 GPa for the intrinsic hardness of the implanted matrix is consistent with this interpretation: if the hardness in the absence of Ti is 7-10 GPa, and if the hardness increment due to Ti is assumed as a first approximation to be 0.5 GPa per at.%, then the predicted hardness for 16 at.% Ti is 15-18 GPa. Moreover, the yield stress which we deduce for the implanted matrix, 5.2 GPa, is correspondingly enlarged from that of the amorphous Fe-Ni alloys.

The substantial strengthening discussed above, coupled with the microstructural homogeneity and the retention of ductility that distinguish amorphous metals, is expected to reduce friction and wear during unlubricated sliding contact. Such hardening should reduces the contact area for interfacial bonding and also increases the resistance to surface fracture, and the microstructural homogenization associated with amorphization should diminish the irregularities that can initiate catastrophic wear. These expectations were born out in earlier tribological studies of steels implanted with Ti and C [5]. Hence, continued exploration of the application this implantation treatment to MEMS materials appears warranted.

ACKNOWLEDGMENTS

Ion-implantation treatments were designed and carried out G. A. Petersen. M. P. Moran prepared TEM specimens and developed surface preparations for mechanical testing. This work was supported by the U.S. Dept. of Energy under Contract DE-AC04-94AL85000. Sandia is a multiprogram laboratory operated by Sandia Corp., a Lockheed Martin Co., for the U.S. Dept. of Energy.

REFERENCES

1. E. W. Becker, W. Ehrfeld, P. Hagmann, A. Maner, and D Münchmeyer, Microelectron. Eng. **4**, 35 (1986).
2 H. Guckel, K. J. Skrobis, J. Klein, and T. R. Christenson, J. Vac. Sci. Technol. A **12**, 2559 (1994).

3. T. R. Christenson and H. Guckel, SPIE Proc. **2639**, 134 (1995).

4. J. A. Knapp, D. M. Follstaedt, and B. L. Doyle, Nucl. Instrum. Methods B **7-8**, 38 (1985).

5. D. M. Follstaedt, Nucl. Instrum. Methods B **10-11**, 549 (1985).

6. D. M. Follstaedt, J. A. Knapp, J. C. Barbour, S. M. Myers, and M. T. Dugger, in Beam Processing of Advanced Materials (ASM, Metals Park, OH, 1996) pp. 77-89.

7. J. Takadoum, J. C. Pivin, J. Chaumont, and C. Roque-Carmes, J. Mater. Sci. **20**, 1480 (1985).

8. M. Nastasi, J.-P. Hirvonen, T. R. Jervis, G. M. Pharr, and W. C. Oliver, J. Mater. Res. **3**, 226 (1988).

9. L. E. Pope, S. T. Picraux, D. M. Follstaedt, J. A. Knapp, and F. G. Yost, J. Mater. for Energy Sys. **7**, 27 (1985).

10. A. W. Mullendore, L. E. Pope, A. K. Hays, G. C. Nelson, C. R. Hills, and B. G. LeFevre, Thin Solid Films **186**, 215 (1990).

11. J. A. Knapp et al., Nucl. Instrum. Methods B, in press.

12. J. A. Knapp et al., Proc. 1996 Fall MRS Meeting, in press.

13. J. F. Ziegler, J. P. Biersack, and U. Littmark, The Stopping and Range of Ions in Solids (Pergamon, New York, 1985).

14. W. C. Oliver and G. M. Pharr, J. Mater. Res. **7**, 1564 (1992).

15. Nanoindentation measurements were carried out by B. Lucas at Nano Instruments Inc., Knoxville, TN.

16. ABAQUS is a product of Hibbitt, Karlsson & Sorensen, Inc., Pawtucket, RI.

17. Atlas of Stress-Strain Curves, edited by H. E. Boyer (ASM, Metals Park, OH, 1987) p. 551.

18. M Hagiwara, in Current Topics in Amorphous Materials: Physics and Technology, edited by Y. Sakurai, Y. Hamakawa, T. Masumoto, K. Shirae, and K. Suzuki (North-Holland, Amsterdam, 1993) pp. 191-195.

19. J. Niebuhr, R. Gerber, A. Schaller, and H.-W. Müller, Physical Data of Amorphous Metals, Part B (Fachinformationszentrum Karlsruhe, Germany, 1991).

20. F. Spaepen, in Physics of Defects, edited by R. Balian, M. Kléman, and J.-P. Poirier (North Holland, Amsterdam, 1981) pp. 133-174.

21. A. Inoue, T. Iwadachi, T. Minemura, and T. Masumoto, Trans. Jap. Inst. Metals **22**, 197 (1981).

DISCLAIMER